Hindawi
Oxidative Medicine and Cellular Longevity
Volume 2021, Article ID 7003861, 12 pages
https://doi.org/10.1155/2021/7003861

Research Article

Thermal Stability Kinetics and Shelf Life Estimation of the Redox-Active Therapeutic and Mimic of Superoxide Dismutase Enzyme, Mn(III) *meso*-Tetrakis(*N*-ethylpyridinium-2-yl)porphyrin Chloride (MnTE-2-PyPCl$_5$, BMX-010)

Clarissa G. C. Maia,[1] **Bárbara C. R. de Araujo**,[2] **Maria B. de Freitas-Marques**,[2] **Israel F. da Costa**,[1] **Maria Irene Yoshida**,[2] **Wagner da Nova Mussel**,[2] **Rita de Cássia O. Sebastião**,[2] **and Júlio S. Rebouças**[1]

[1]*Departamento de Química, Centro de Ciências Exatas e da Natureza, Universidade Federal da Paraíba, João Pessoa, PB 58051-900, Brazil*
[2]*Departamento de Química, Instituto de Ciências Exatas, Universidade Federal de Minas Gerais, Belo Horizonte, MG 31207-901, Brazil*

Correspondence should be addressed to Rita de Cássia O. Sebastião; ritacos@gmail.com and Júlio S. Rebouças; jsreboucas@quimica.ufpb.br

Received 2 June 2021; Accepted 12 November 2021; Published 6 December 2021

Academic Editor: Grzegorz Wegrzyn

Mn(III) *meso*-tetrakis(*N*-ethylpyridinium-2-yl)porphyrin chloride (MnTE-2-PyPCl$_5$, BMX-010, and AEOL10113) is among the most studied superoxide dismutase (SOD) mimics and redox-active therapeutics, being currently tested as a drug candidate in a phase II clinical trial on atopic dermatitis and itch. The thermal stability of active pharmaceutical ingredients (API) is useful for estimating the expiration date and shelf life of pharmaceutical products under various storage and handling conditions. The thermal decomposition and kinetic parameters of MnTE-2-PyPCl$_5$ were determined by thermogravimetry (TG) under nonisothermal and isothermal conditions. The first thermal degradation pathway affecting Mn-porphyrin structural integrity and, thus, activity and bioavailability was associated with loss of ethyl chloride via *N*-dealkylation reaction. The thermal stability kinetics of the *N*-dealkylation process leading to MnTE-2-PyPCl$_5$ decomposition was investigated by using isoconversional models and artificial neural network. The new multilayer perceptron (MLP) artificial neural network approach allowed the simultaneous study of ten solid-state kinetic models and showed that MnTE-2-PyPCl$_5$ degradation is better explained by a combination of various mechanisms, with major contributions from the contraction models R1 and R2. The calculated activation energy values from isothermal and nonisothermal data were about 90 kJ mol^{-1} on average and agreed with one another. According to the R1 modelling of the isothermal decomposition data, the estimated shelf life value for 10% decomposition ($t_{90\%}$) of MnTE-2-PyPCl$_5$ at 25°C was approximately 17 years, which is consistent with the high solid-state stability of the compound. These results represent the first study on the solid-state decomposition kinetics of Mn(III) 2-*N*-alkylpyridylporphyrins, contributing to the development of this class of redox-active therapeutics and SOD mimics and providing supporting data to protocols on purification, handling, storage, formulation, expiration date, and general use of these compounds.

1. Introduction

Water-soluble, cationic Mn(III) porphyrins derived from the 2-*N*-pyridylporphyrin scaffold were originally developed as potent superoxide dismutase (SOD) mimics, peroxynitrite scavengers, and later proven to be efficient redox-active therapeutics [1–6]. Two lead compounds, Mn(III) *meso*-tetrakis(*N*-ethylpyridinium-2-yl)porphyrin chloride (MnTE-2-PyPCl$_5$, also known as BMX-010) [2] and Mn(III) *meso*-tetrakis(*N*-n-butoxyethylpyridinium-2-yl)porphyrin chloride (MnTnBuOE-2-PyPCl$_5$, also known as BMX-001) [7, 8], were found to be safe and well tolerated in phase I clinical trials [1, 9–13]. Whereas MnTE-2-PyPCl$_5$ progressed to various phase II clinical trials on atopic dermatitis and itch, the MnTnBuOE-2-PyPCl$_5$ analogue, which was developed based on the MnTE-2-PyPCl$_5$ prototype, is now being investigated in four phase II clinical trials as radioprotectors for glioma, head and neck cancer, multiple brain metastases, and anal squamous cell carcinoma [1, 10, 11, 14].

MnTE-2-PyPCl$_5$ has an established reputation of being the Mn(III) 2-*N*-alkylpyridylporphyin-based prototype for the design of bioavailable SOD mimics, the development of catalytic antioxidants, and mechanistic studies [1, 3, 12, 15–17]. Given its safe toxicity profile in animal models and humans [1, 9, 10, 13], MnTE-2-PyPCl$_5$ is usually the compound of choice in most exploratory preclinical studies [12, 17–25], being forwarded to translational medicine and clinical trials [1, 9, 10], and is now recognized as an excellent redox-active therapeutic [1], with well-defined pharmacokinetics [26, 27]. Despite the large number of studies dedicated to unravelling the biological and clinical aspects of MnTE-2-PyPCl$_5$ both in vitro and in vivo [1, 16–18, 22], studies on the stability of this class of compounds are still somewhat limited [28–30]. It is worth noting, however, that information on MnTE-2-PyPCl$_5$ stability may shed light on the stability of other MnP analogues [28] and likely support protocols on purification, handling, storage, formulation, expiration date, and general use of these compounds [31–34].

As a characteristic of Mn-porphyrins in general, MnTE-2-PyPCl$_5$ with Mn in the +3 oxidation state is extremely stable against acid solvolysis: Mn(III) demetallation is difficult even under concentrate H_2SO_4 conditions [2]. MnTE-2-PyPCl$_5$ is relatively stable against oxidative degradation under biological conditions, particularly the presence of many reactive substrates or biological sacrificial reductors [35]. Not only do Mn-porphyrins withstand major reactive oxygen and nitrogen species (ROS/RNS) but also H_2O_2 is a key molecule in the therapeutic effects of Mn-porphyrins, as clearly shown by Jaramillo et al. [36] and recently summarized elsewhere [1]. Whereas MnTE-2-PyPCl$_5$ undergoes some bimolecular degradation when incubated with net H_2O_2 [22, 29], decomposition by peroxides is not at all an issue for solid-state/aqueous solution storage and/or general formulation of this compound [28]. The thermal degradation of MnTE-2-PyPCl$_5$, as a representative of the Mn(III) 2-*N*-alkylpyridylporphyrin class, has been addressed in a single thermogravimetric study so far [28]. The thermal behavior of MnTE-2-PyPCl$_5$ salts under aerobic conditions is characterized by three events: (i) dehydration of associated water molecules (room temperature to 134°C), (ii) *N*-dealkylation via loss of ethyl chloride (134–279°C) to yield MnT-2-PyPCl (see Figure 1), and (iii) various overlapping porphyrin-ring decomposition processes to yield manganese oxides as combustion residues (279–950°C) [28]. As MnTE-2-PyPCl$_5$ is often administered as aqueous formulations by various routes (e.g., intraperitoneal, subcutaneous, intravenous, and oral) [17, 26, 27], MnP intrinsic biological activity on the Mn basis is not affected by reversible dehydration [28]. Conversely, *N*-dealkylation of MnTE-2-PyPCl$_5$ changes the porphyrin structure irreversibly, reducing the overall charge of the molecule, which affects Mn(III)/Mn(II) redox potential, electrostatic facilitation for superoxide/peroxynitrite approach/scavenging, reactions with protein thiolates, and MnTE-2-PyP^{5+}(aq) pharmacological activity [1, 17, 37, 38].

Thermogravimetric (TG) analyses are important for the evaluation and/or comparison of thermal stabilities of pharmaceutical materials, the study of drug-excipient compatibility in drug products, and the determination of kinetic parameters associated with thermal processes (such as activation energies, frequency factor, and reaction order) [31–34, 39, 40]. Overall, this information is useful for the development of pharmaceutical products and quality control [32, 34, 39, 41]. Studies on the kinetics of thermal degradation are recommended to evaluate the thermal stability of active pharmaceutical ingredients (API) and/or their solid-state pharmaceutic formulations [31–34, 39, 41, 42]. These kinetic studies are often carried out in the pharmaceutic field by nonisothermal (dynamic) or isothermal thermogravimetric analyses [43–49]. Kinetic studies under isothermal TG conditions are particularly relevant as they are amenable to Arrhenius equation treatment and make possible the estimation of room temperature degradation rate from extrapolation of accelerated, experimental, high-temperature degradation rates [34, 42]. These kinetic studies are particularly useful to provide reliable estimates of the shelf life of pharmaceutical products under various storage and handling conditions [31, 34].

We describe herein the first study on the kinetics of thermal degradation of MnP-based redox-active therapeutics under isothermal and nonisothermal conditions. Additionally, it is worth noting that thermal decomposition kinetic models were evaluated using a state-of-the-art approach, based on the multilayer perceptron (MLP) artificial neural network [48–52]. MnTE-2-PyPCl$_5$ was chosen as a representative API of the class of Mn(III) 2-*N*-alkylpyridylporphyrins, currently developed as SOD mimics, biomimetic models, catalytic antioxidants, and redox-active therapeutics.

2. Materials and Methods

MnTE-2-PyPCl$_5$ and the nonalkylated analogue MnT-2-PyPCl (see Figure 1) were prepared and purified as previously reported [2, 53] and showed characterization features consistent with published data [28, 53–55]. Although these compounds are usually labeled as anhydrous species (i.e., MnTE-2-PyPCl$_5$), the isolated solids often contain variable amounts of water molecules, depending on sample workup,

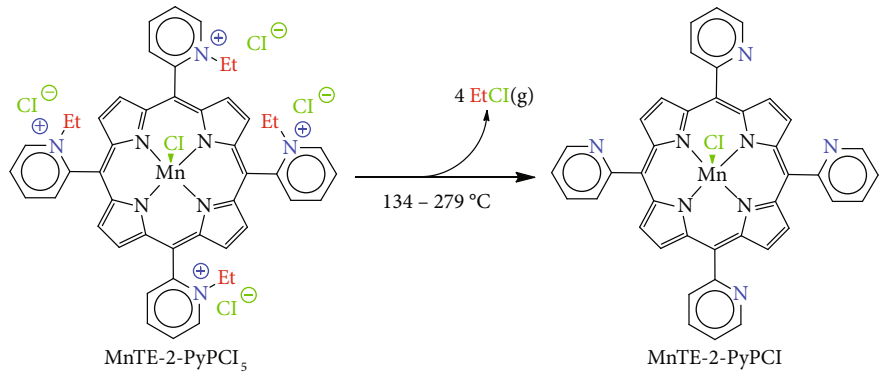

Figure 1: Thermal *N*-dealkylation of MnTE-2-PyPCl$_5$ under dynamic air during thermogravimetric analysis at a heating rate of 10°C/min.

handling, and storage [28]. In this work, the cationic MnP, MnTE-2-PyPCl$_5$, contained 8 molecules of water, whereas the neutral MnP, MnT-2-PyPCl, was analyzed as an anhydrous species, according to thermogravimetric data (see below). All samples were investigated by simultaneous thermogravimetric and differential thermal analyses (TG/DTA) under isothermal and nonisothermal conditions. The experimental kinetic designs described below for these two conditions of analyses agree with the International Confederation for Thermal Analysis and Calorimetry (ICTAC) recommendations [45–47].

2.1. Thermal Analysis. TG curves were obtained on a Shimadzu DTG60 thermal analyzer using 2–3 mg samples, accurately weighed in alumina crucibles directly in the thermobalance, under a dynamic atmosphere of synthetic air with a flow rate of 50 mL min^{-1}.

For the kinetic studies, various TG curves were registered independently using heating rates of 5, 7.5, 10, and 12.5°C min^{-1} in the temperature range from 30 to 600°C for nonisothermal experiments. Isothermal experiments were carried out at 158, 160, 162, and 164°C for a period of 60 minutes; in these experiments, the samples were heated from room temperature to the target isothermal temperature with a heating rate of 10°C min^{-1}.

2.2. Kinetic Study Using the Vyazovkin Isoconversional Method in Nonisothermal TG Data. The solid-state decomposition process follows the general first-order kinetic equation:

$$\frac{d\alpha}{dT} = k(T)f(\alpha), \tag{1}$$

with $k(T)$ as the rate constant following the Arrhenius equation and $f(\alpha)$ as the reaction model, with α as the conversion degree; $\alpha = (m_0 - m_t)/(m_0 - m_f)$, where m_0 is the initial sample mass, m_f is the final sample mass, and m_t is the sample mass at time t.

Assuming $\beta_i (i = 1, \cdots, n)$ as the heating rate, the temperature integral $I(E, T) = \int_0^T \exp(-E_\alpha/\mathrm{RT})dt$, and $(\alpha) = \int_0^\alpha [f(\alpha)]^{-1} d\alpha$, the general equation (1) can be rewritten as

$$g(\alpha) = \frac{A}{\beta} I(E, T). \tag{2}$$

The isoconversional Vyazovkin [44] method assumes that the reaction model is independent of the heating rate; for this, we have for a given conversion

$$\left(\frac{A_\alpha}{\beta_1}\right) I(E_\alpha, T_{\alpha 1}) = \left(\frac{A_\alpha}{\beta_2}\right) I(E_\alpha, T_{\alpha 2}) = \cdots = \left(\frac{A_\alpha}{\beta_n}\right) I(E_\alpha, T_{\alpha n}). \tag{3}$$

The frequency factor, A_α, is considered constant for the processes submitted to small variation of the heating rate, so this equation can be treated considering the following optimization:

$$\sum_{i=1}^{n} \sum_{j \neq 1}^{n} \frac{\mathrm{I}(E_\alpha, T_{\alpha 1})\beta_j}{\mathrm{I}(E_\alpha, T_{\alpha 1})\beta_i} = \text{minimum}. \tag{4}$$

The temperature integral can be solved assuming the following approximation [56]:

$$\int_0^T \exp\left(\frac{-E}{\mathrm{RT}}\right) dT = \frac{E}{R} \int_\infty^x \frac{\exp(-x)}{x^2} dx = \frac{E}{R} p(x), \tag{5}$$

with $x = E/RT$ and $p(x)$ calculated using the Senum-Yang approximation [56] of the third degree:

$$p(x) = \frac{\exp(-x)}{x} \frac{x^2 + 10x + 18}{x^3 + 12x^2 + 368x + 24}. \tag{6}$$

The percentage error of the $p(x)$ function for the 3$^{\mathrm{rd}}$ rational approximation is about 10^{-5} percent [56].

2.3. Kinetic Study Using the MLP Neural Network in Isothermal TG Data. The MLP neural network applied in this study was proposed initially by Sebastião et al. [48–50]. The architecture of this MLP has only one artificial neuron in the input and output layers. The intermediate layer, however, has ten artificial neurons, according to the number of kinetic models considered in the process of the

Table 1: Kinetic models used in the multilayer perceptron (MLP) neural network for evaluating MnTE-2-PyPCl$_5$ isothermal decomposition [43].

Kinetic model	Kinetic equation	Model type
F1	$-\ln(1-\alpha) = kt + k_0$	Chaotic nucleoid
Am	$[-\ln(1-\alpha)]^{1/m} = kt + k_0$, with $m = 2, 3, 4 \cdots$	Avrami-Erofeev
Au	$\dfrac{\ln \alpha}{(1-\alpha)} = kt + k_0$	Avrami-Erofeev
R1	$\alpha = kt + k_0$	Linear contraction
R2	$1-(1-\alpha)^{1/2} = kt + k_0$	Area contraction
R3	$1-(1-\alpha)^{1/3} = kt + k_0$	Volume contraction
D1	$\alpha^2 = kt + k_0$	One dimension
D2	$(1-\alpha)\ln(1-\alpha) + \alpha = kt + k_0$	Two dimensions
D3	$\left[1-(1-\alpha)^{1/3}\right]^2 = kt + k_0$	Three dimensions
D4	$1 - \dfrac{2}{3}\alpha - (1-\alpha)^{2/3} = kt + k_0$	Ginstling-Brounshtein

thermal solid decomposition. Table 1 presents the kinetic models studied.

The states of neurons o_k are defined as

$$o_k = f\left(\sum_{j=0}^{m} w_{kj} x_k\right), \tag{7}$$

with x_k being the state of the artificial neuron in the previous layer and w_{kj} being the weights between the neurons k and j. In this particular type of network, there are also weights called bias, w_{i0}, defined as unity parameters to amplify or reduce the linear correlation of the network [48, 49].

In this proposed architecture of MLP, the weights w_{i1} and the bias w_{i0} were predetermined from the fit of experimental data by each kinetic model in each studied temperature, where the weights are the rate constants and linear coefficient of the kinetic models. These weights do not change in the learning process of the network and can be represented assuming a weight matrix w_1 as

$$w_1 = \begin{pmatrix} w_{21} & w_{20} \\ w_{31} & w_{30} \\ w_{41} & w_{40} \\ w_{51} & w_{51} \\ \vdots & \vdots \\ w_{n1} & w_{n0} \end{pmatrix}. \tag{8}$$

Assuming x to be the experimental time data for each studied temperature,

$$x = \begin{pmatrix} t \\ 1 \end{pmatrix}. \tag{9}$$

In this case, the $w_1 x$ matrix calculates the state of the artificial neurons in the intermediate layer $W_1 x$:

$$w_1 x = \begin{pmatrix} w_{21} t + w_{20} \\ w_{31} t + w_{30} \\ w_{41} t + w_{40} \\ w_{51} t + w_{50} \\ \vdots \\ w_{n1} t + w_{n0} \end{pmatrix}. \tag{10}$$

The neurons in the intermediate layer must be activated by an activation function, f, to send out information to the output layer. From this, their states are defined by

$$o_k = f(w_1 x). \tag{11}$$

The activation functions should assume a predetermined value; generally, $f(x) = 0$ before calculating the state of neurons; activate the neurons assuming values near to the unity and making sure this is a increasing function $df(x)/dx \geq 0$, to warranty the energy function optimization [49]. If we chose a linear activation function in the output layer, the network response, given by the state of the neuron in the output layer, is

$$o_k = w_2 f(w_1 x), \tag{12}$$

with W_2 being the interconnection weight vector of the output layer.

The MLP learning process consists of an energy function optimization, from which only the w_2 vector has to be

determined [49]. Considering α_{exp} as the experimental data, this energy function is

$$E = \left\| w_2 f(w_1 x) - \alpha_{exp} \right\|_2^2. \quad (13)$$

To solve this equation, the w_2 contribution of each kinetic model to describe the experimental data can be calculated by the well-known pseudo-inverse algorithm [49]

$$w_2 = \left(B^T B\right)^{-1} B^T \alpha_{exp}, \quad (14)$$

with $B = f(w_1 x)$.

3. Results and Discussion

3.1. Thermal Decomposition of MnTE-2-PyPCl$_5$. In our previous studies on the thermal stability of MnTE-2-PyPCl$_5$ [28], we established that the thermogravimetric events of this Mn-porphyrin under dynamic air were associated with three major processes: (i) dehydration, (ii) *N*-dealkylation, and (iii) organic matter degradation to yield Mn oxide as the final residue at 900 or 950°C. The *N*-dealkylation reaction of MnTE-2-PyPCl$_5$ during the thermogravimetric analyses under air at a heating rate of 10°C min^{-1} takes place between 134 and 279°C (see Figure 2). The loss of ethyl chloride (EtCl) was characterized by gas chromatography-mass spectrometry (GC-MS) of the evolved gas (EtCl) and by characterization of the residue at 279°C, which was consistent with MnT-2-PyPCl (see Figure 1) by spectroscopic and chromatographic analyses [28]. Additionally, thermogravimetric analysis of an analytical sample of MnT-2-PyPCl with no *N*-alkyl moieties (prepared independently [53]) showed no major events in the temperature range associated with EtCl loss in MnTE-2-PyPCl$_5$ (see Figure 2; see also Figures S1 and S2 and Tables S1 and S2 in Supplementary Materials for complementary data by derivative thermogravimetry (DTG) and differential thermal analysis (DTA)). Whereas dehydration is a reversible process, the *N*-dealkylation of MnTE-2-PyPCl$_5$ to yield MnT-2-PyPCl (see Figure 1) represents the first irreversible thermal event that compromises the MnP structural integrity, affecting permanently its catalytic efficiency, lipophilicity, bioavailability, and expected therapeutic outcome [17, 28, 38, 54]. Thus, understanding the kinetics of the MnTE-2-PyPCl$_5$ thermal *N*-dealkylation process may prove useful to provide researchers and the pharmaceutic industry with information on handling/storage of MnTE-2-PyPCl$_5$, shelf life, and usage. Commercially impure samples of Mn(III) 2-*N*-alkylpyridylporphyrins, containing a mixture of partially *N*-dealkylated compounds most likely derived from inadequate thermal workup procedures [38, 54], have already clouded some biological conclusions on the in vivo SOD activity of these Mn-porphyrins [54, 57].

The kinetic studies on the thermal *N*-dealkylation of MnTE-2-PyPCl$_5$ were carried out by nonisothermal and isothermal protocols as presented below, observing the recommendations of the International Confederation for Thermal Analysis and Calorimetry (ICTAC) [45, 47]. The specific temperature ranges for the kinetic studies were chosen based on the interval in which only the *N*-dealkylation process of MnTE-2-PyPCl$_5$ is prevalent (see Figure 2) [54]. Although thermal kinetic data are usually collected at high temperature under accelerated thermal degradation conditions, the isothermal results may be extrapolated to lower temperatures using the Arrhenius equation, to provide estimates of drug thermal stability under different target temperatures of interest to handling and storage associated with good manufacturing practices [34, 42, 58].

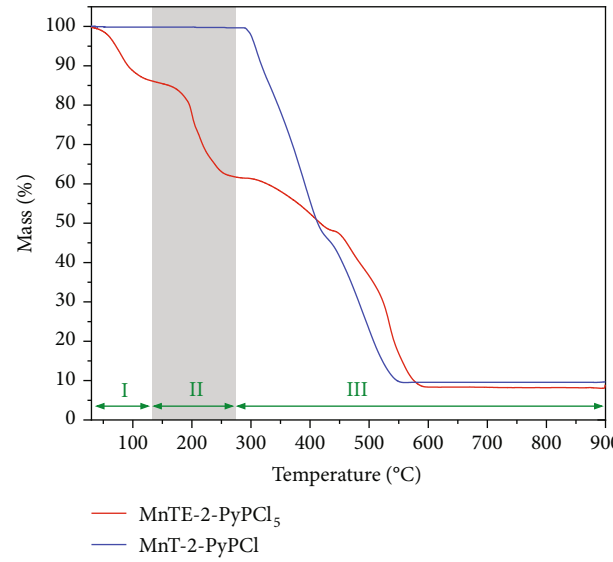

Figure 2: Thermogravimetric curve for MnTE-2-PyPCl$_5$ (red trace, formally MnTE-2-PyPCl$_5$·8H$_2$O) and MnT-2-PyPCl (blue trace) under dynamic air at a heating rate of 10°C min^{-1}. Thermal processes correspond to the following: I—dehydration; II—*N*-dealkylation; and III—porphyrin ring decomposition to yield Mn oxides. Corresponding data for the nonalkylated sample MnT-2-PyPCl (blue trace) is presented as a control, indicating no *N*-dealkylation process in the highlighted 134–279°C temperature range. DTG and DTA curves are included as Figures S1 and S2 in Supplementary Materials.

3.2. Nonisothermal Kinetic Analysis. The decomposition process associated with MnTE-2-PyPCl$_5$ thermal *N*-dealkylation under nonisothermal conditions was investigated. From this methodology, the kinetic parameters of activation energy (E_a) and frequency factor (A) were determined according to the conversion degree (α). The nonlinear isoconversional method proposed by Vyazovkin et al. [45] was used. This method allows an indirect analysis of multistep processes, considering the activation energy as a function of the conversion degree.

Figure 3 shows the nonisothermal experimental data obtained from the four heating rates chosen to follow the MnTE-2-PyPCl$_5$*N*-dealkylation process: 5.0, 7.5, 10.0, and 12.5°C min^{-1}. The curves are not overlapped, and observe the ICTAC recommendations for kinetic studies [45–47]. These curves were treated by the nonlinear Vyazovkin method, and Figure 4 shows the activation energy

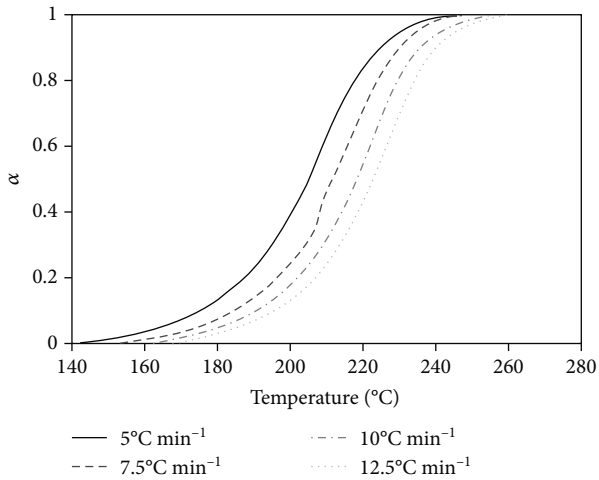

Figure 3: Nonisothermal curves for MnTE-2-PyPCl$_5$ thermal decomposition.

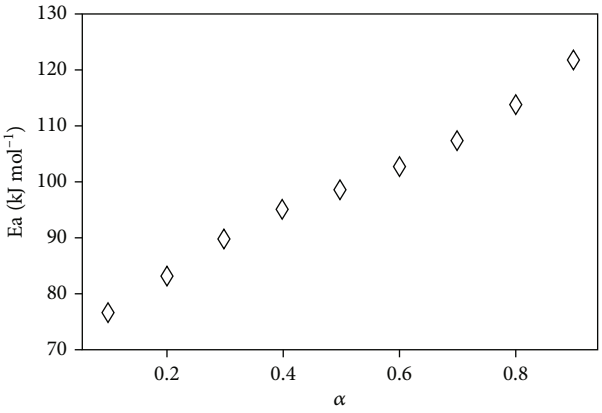

Figure 4: Activation energy according to the extent of conversion determined by the Vyazovkin method for the MnTE-2-PyPCl$_5$ thermal *N*-dealkylation.

determined for the thermal decomposition process of MnTE-2-PyPCl$_5$, as a function of the conversion degree. Figure 4 reveals that the activation energy increases as the conversion proceeds, starting from 75 kJ mol^{-1} at the beginning of the process, reaching 100 kJ mol^{-1} at $\alpha = 0.5$, and finishing with values of 125 kJ mol^{-1}. These high activation energies not only indicate but also are consistent with the observed high thermal stability of the compound [28]. The standard deviations for the Vyazovkin adjustments are presented in Table 2, and their small values warranty that the Vyazovkin method was used properly to treat the MnTE-2-PyPCl$_5$ thermal *N*-dealkylation data. It is worth noting that the activation energy represents the energy necessary to initiate the MnTE-2-PyPCl$_5$ decomposition.

3.3. Isothermal Kinetic Analysis by the MLP Artificial Neural Network. Isothermal decomposition of solids generally occurs at the product-reagent interface [44], being described by kinetic models well established in the literature [48–50].

Table 2: Standard deviation to the Vyazovkin method according to conversion (α) for the MnTE-2-PyPCl$_5$ thermal *N*-dealkylation.

α conversion	Standard deviation/10^{-3}
0.10	1.1930
0.20	1.5438
0.30	2.8396
0.40	4.2336
0.50	1.5133
0.60	4.5673
0.70	3.3551
0.80	2.1008
0.90	3.8991

These models correlate the decomposition fraction, $\alpha(t)$, with time at chosen appropriate temperatures. An adapted multilayer perceptron (MLP) neural network algorithm was developed by our group [48, 49] as a homemade algorithm using the MATLAB language [50, 51]. The algorithm is different from traditional MLP approaches as it does not vary the interconnection weights between the input and intermediate layers. In this MLP approach, only the weights between the intermediate and output layers are optimized, which provides the contribution of each kinetic model in the experimental data description.

In the current study, a total of 12 kinetic models (see Table 1) were investigated simultaneously, out of which 10 models (i.e., D1, D2, D3, D4, R1, R2, R3, Am2, Am4, and Au) were found to describe in a combined manner the thermal decomposition kinetics associated with MnTE-2-PyPCl$_5$ thermal *N*-dealkylation reaction. The curves of decomposition fraction, $\alpha(t)$, for MnTE-2-PyPCl$_5$ isothermal experiments at 158, 160, 162, and 164°C are presented in Figure 5 along with the MLP adjustment considering ten kinetic models for the decomposition process. As shown in Figure 5, the residual error of the MLP adjustment in all cases is about 10^{-4}, attesting the robustness of the method.

The MLP neural network approach is exceptionally accurate compared to the adjustment of each individual kinetic model separately. Figure 6 presents the residual error of each kinetic model considered individually to fit the experimental data. It is worth noting that fitting of experimental data with various kinetic models resulted in comparable residual errors, many of which are of the same order of magnitude (see Figure 6). This result strongly suggests that the *N*-dealkylation of MnTE-2-PyPCl$_5$ via a thermal decomposition process is better understood as an overlapping contribution of many mechanisms combined [48, 49]; for this case, the R1, R2, Am2, and Am4 mechanisms presented smaller residual error to fit the experimental data. Nonetheless, the contraction models R1 and R2 explain the experimental data with more accuracy. The R2 model assumes the nucleation occurring rapidly on the surface of the crystal, which presents a cylinder shape. In this kinetic model, that accounts for a contracting area; the radius contraction follows $r = r_0 - kt$, where r is the radius at time t, r_0 is the initial radius, and

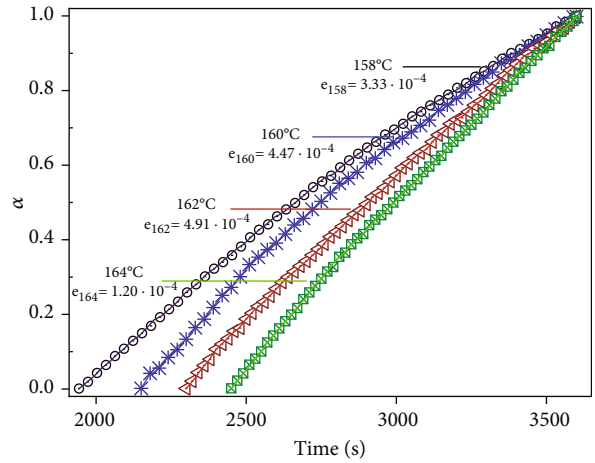

Figure 5: Decomposition fraction of MnTE-2-PyPCl$_5$, $\alpha(t)$, as a function of time (t) at 158, 160, 162, and 164°C. Symbols are for experimental data, and the solid line is for MLP results. The residual errors (e) of the MLP adjustments at each temperature analyzed are also presented.

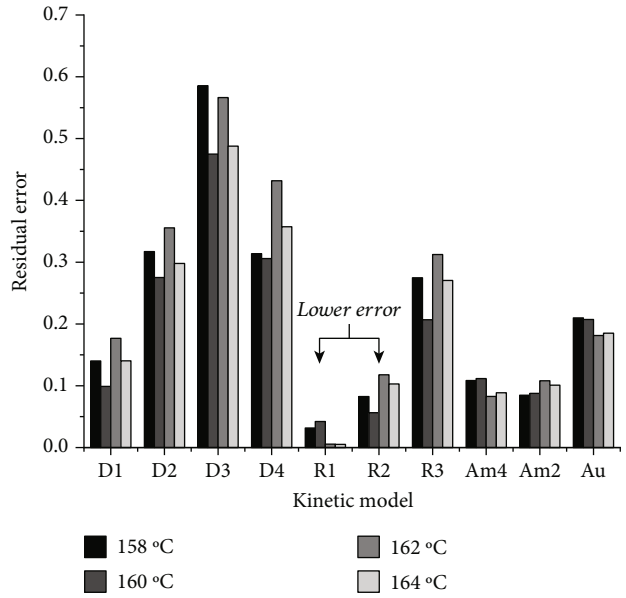

Figure 6: Residual errors for the adjustment of the isothermal experimental data on MnTE-2-PyPCl$_5$*N*-dealkylation to each kinetic model individually.

k is the rate constant, as schematically represented in Figure 7. The generalized Rn models, which encompass R1 and R2, are mathematical functions that describe reactions taking place in the boundary phase, with diffusion processes being extremely fast, which prevents an adequate interaction of reactants in the interface [41, 59]. These phase boundary-controlled reaction processes are, thus, controlled by the rearrangement of the reactants in the limitrophe phase. The Rn models are known as geometrical contraction models, but R1 is similar to the ones usually applied to

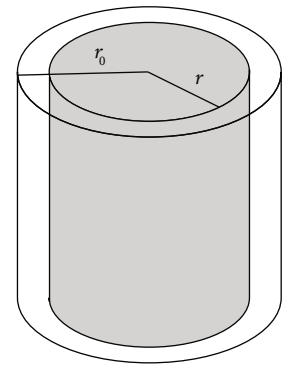

Figure 7: Geometrical contraction of cylinder crystals that presents the R2 kinetic mechanism.

describe the reaction order mechanisms in a homogeneous system, following a zero-order reaction rate.

In the MLP artificial neutral network approach, ten kinetic models (i.e., D1, D2, D3, D4, R1, R2, R3, Am2, Am4, and Au, see Table 1) were considered simultaneously in the intermediate layer, with the w_1 matrix (equation (8)) determined by the rate constant (k) and linear coefficient ($k0$) of kinetic models by the fitting experimental data of each isothermal curve. The contribution of the kinetic models to the MnTE-2-PyPCl$_5$ isothermal decomposition process is presented in Figure 8, which reveals that for all studied temperatures (158, 160, 162, and 164°C), the most significant contributions were those associated with the contraction models R1 and R2. Thus, the contraction models R1 and R2 showed both smaller error and greater contribution in describing the phenomenon of MnTE-2-PyPCl$_5$ thermal decomposition.

The rate constants determined by the experimental data adjustment into the kinetic models via the MLP neural network approach (w_1 matrix, equation (8)) were used to calculate the activation energy of MnTE-2-PyPCl$_5$ thermal decomposition. The MLP-derived values shown in Figure 9 are comparable to the activation energies calculated using the Vyazovkin method (see Figures 4 and 9). This agreement with the nonisothermal result indicates that the decomposition process is not affected by the experimental condition (i.e., isothermal or nonisothermal protocol) and, again, the MLP values of activation energy are consistent with the overall stability of MnTE-2-PyPCl$_5$.

MnTE-2-PyPCl$_5$ is often stored as a nonformulated solid or as aqueous solution formulations [9], [10, 17]. Nonformulated solid MnTE-2-PyPCl$_5$ has often been stored at room temperature, presumably between 15 and 35°C [9, 10, 28]. Thus, considering the activation energy values and rate constants determined at high temperature, the kinetic parameters at 25°C were estimated, using the Arrhenius equation. These kinetic data also allowed the estimation of the $t_{90\%}$ shelf life value for MnTE-2-PyPCl$_5$ (i.e., the time in which the initial MnP concentration decays by 10%) at 25 and 158°C (see Table 3). The $t_{90\%}$ value is an important parameter that is recommended for estimating the API shelf life [34, 60]. As the model R1 showed smaller error and

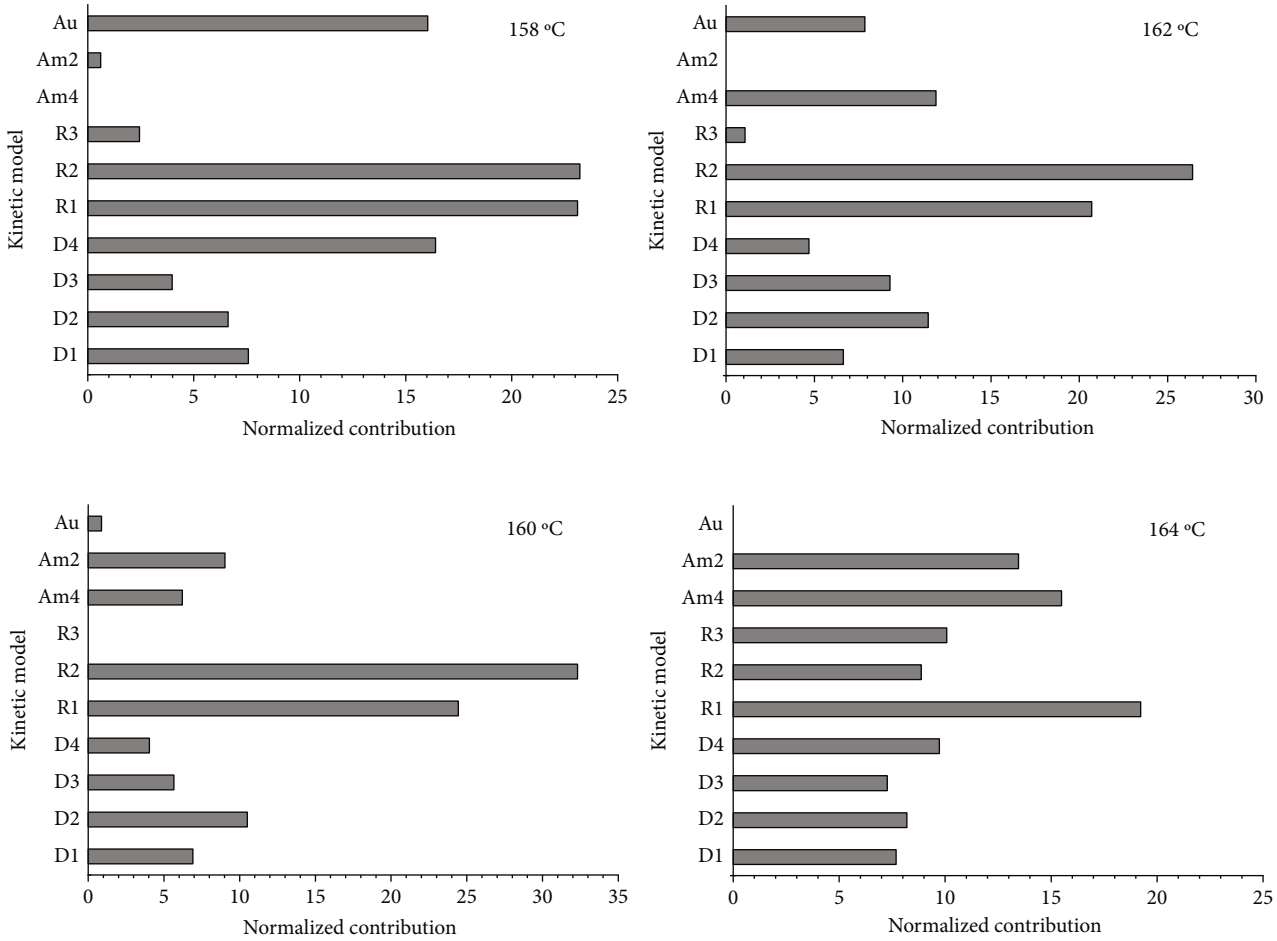

Figure 8: Kinetic model contributions to the description of the MnTE-2-PyPCl$_5$ isothermal decomposition processes at 158, 160, 162, and 164°C (normalized values) as determined by the MLP artificial neutral network approach.

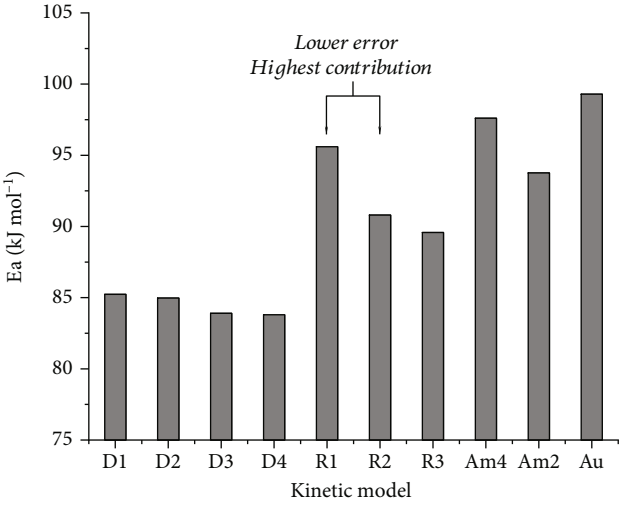

Figure 9: Activation energy (E_a) determined by the multilayer perceptron (MLP) artificial neural network for MnTE-2-PyPCl$_5$ thermal decomposition.

greater contribution to the phenomenon of thermal decomposition of the material, the $t_{90\%}$ value found by this model is the most adequate to describe the behavior of MnTE-2-PyPCl$_5$ over time. Therefore, it is expected that it would take nearly 17 years for solid MnTE-2-PyPCl$_5$ to reach a 10% *N*-dealkylation at 25° C, which is consistent with the high stability empirically observed for this compound on daily routine handling and storage in the laboratory [54]. Of note, a solid sample of high-purity MnTE-2-PyPCl$_5$ stored in a closed vial at room temperature in the dark for 7 years in our laboratories showed no noticeable signs of *N*-dealkylation when analyzed by thin-layer chromatography (data not shown). As shelf life values may be significantly affected by storage and drug formulations (including the nature of excipients) [34, 52, 60], the calculated $t_{90\%}$ value for MnTE-2-PyPCl$_5$ is valid if the net solid material is kept in ideal conditions of humidity. As noted, MnTE-2-PyPCl$_5$ is a hydratable molecule. The presence of humidity can trigger hydrolytic processes. High humidity generates absorption of the excess moisture in the air, which can be just as destructive as environments with low humidity. A humidity excess can compromise potency and effectiveness, leading to degradation or even toxicity in some products. It may promote the

Table 3: Activation energy (E_a), frequency factor as ln (A), and time to which the concentration decays by 10% ($t_{90\%}$ shelf life value), determined by the multilayer perceptron (MLP) artificial neural network for MnTE-2-PyPCl$_5$ thermal decomposition at 158 and 25°C.

Kinetic model	E_a (kJ mol^{-1})	ln (A)	$t_{90\%}$ at 158°C (h)	$t_{90\%}$ at 25°C (years)
D1	85.2302	17.3056	59.4421	5
D2	84.9668	16.1542	69.1946	5
D3	83.9006	15.1482	141.75	9
D4	83.8007	14.5778	242.58	16
R1	95.5999	19.2077	62.05	17
R2	90.7974	17.6960	74.48	11
R3	89.5753	17.1541	91.42	12
Am4	97.6001	19.6486	69.58	25
Am2	93.7599	19.1985	37.77	8
Au	99.2897	22.0898	9.70	4

growth of microorganisms, compromising their biological integrity. The International Conference on Harmonization (ICH) in the topic Q1 A(R2) deals with the stability testing of new drugs and products, delimiting good practices of manipulation and storage concerning temperature and humidity parameters. Those variables take into account the country climate zone classification. MnTE-2-PyPCl$_5$ must be stored in a hermetically sealed flask and kept at a storage temperature of 30°C ± 2°C and relative humidity of 75% ± 5% whereas Brazil belongs to climate zone IV [61, 62]. It is worth noting that these data drive further studies on MnTE-2-PyPCl$_5$ formulations and stability.

4. Conclusions

The first study on the thermal stability kinetics of Mn(III) 2-*N*-alkylpyridylprophyrin was carried out with the prototypical MnTE-2-PyPCl$_5$ compound using thermogravimetry (TG) under nonisothermal and isothermal conditions. The new multilayer perceptron (MLP) artificial neural network approach allowed the simultaneous study of ten solid-state kinetic models and showed that *N*-dealkylation associated with MnTE-2-PyPCl$_5$ degradation is better explained by a combination of various mechanisms, with major contributions from the contraction models R1 and R2. The calculated activation energy values from isothermal and nonisothermal data agreed with one another and were consistent with the observed high thermal stability of MnTE-2-PyPCl$_5$ in the solid state. The $t_{90\%}$ shelf life value at 25°C estimated from the isothermal decomposition data was approximately 17 years. These results contribute to the development of this class of redox-active therapeutics and SOD mimics and provide supporting data to protocols on purification, handling, storage, formulation, expiration date, and general use of these compounds.

Additionally, these MnTE-2-PyPCl$_5$ results not only set the grounds for studying other Mn(III) porphyrin-based SOD mimics and redox-active therapeutics but also represent a first approximation to the thermal stability kinetic parameters of the chemically related Zn(II) porphyrin counterpart, ZnTE-2-PyPCl$_4$, and its Zn(II) 2-*N*-alkylpyridylporphyrin analogues, which are being actively pursued as efficient and selective photosensitizers for antimicrobial photodynamic inhibition (aPDI) [63–67].

Data Availability

The data used to support the findings of this study are available from the corresponding author upon request.

Conflicts of Interest

The authors declare that there is no conflict of interest regarding the publication of this paper.

Acknowledgments

C.G.C.M and B.C.L.A acknowledge the PhD scholarships by CNPq and CAPES, respectively. We thank Dr. Victor Hugo A. Pinto and Dr. Jacqueline C. Bueno-Janice for the analyses of a 7-year-old sample of MnTE-2-PyPCl$_5$. J.S.R dedicates this paper to the memory of Dr. Margaret Tome who greatly advanced our current understanding on the biological modes of action of MnTE-2-PyPCl$_5$ and MnP-based redox-active therapeutics. This study was funded by the Coordenação de Aperfeiçoamento de Pessoal de Nível Superior (CAPES), Conselho Nacional de Desenvolvimento Científico e Tecnológico (CNPq), Fundação de Amparo à Pesquisa do Estado de Minas Gerais (FAPEMIG), Financiadora de Estudos e Projetos (FINEP), and Universidade Federal da Paraíba (UFPB).

Supplementary Materials

The thermogravimetry (TG), derivative thermogravimetry (DTG), and differential thermal analyses (DTA) were provided for both MnTE-2-PyPCl$_5$ and MnT-2-PyPCl samples. *(Supplementary Materials)*

References

[1] I. Batinic-Haberle, A. Tovmasyan, Z. Huang et al., "H_2O_2-driven anticancer activity of Mn porphyrins and the underlying molecular pathways," *Oxidative Medicine and Cellular Longevity*, vol. 2021, 23 pages, 2021.

[2] I. Batinić-Haberle, I. Spasojević, P. Hambright, L. Benov, A. L. Crumbliss, and I. Fridovich, "Relationship among redox potentials, proton dissociation constants of pyrrolic nitrogens, and in vivo and in vitro superoxide dismutating activities of manganese(III) and iron(III) water-soluble porphyrins," *Inorganic Chemistry*, vol. 38, no. 18, pp. 4011–4022, 1999.

[3] C. Policar, "Mimicking SOD, why and how: bio-inspired manganese complexes as SOD mimic," in *Redox-Active Therapeutics*, I. Batinic-Haberle, J. S. Rebouças, and I. Spasojevic, Eds., pp. 125–164, Cham, Springer, 2016.

[4] L. M. Slosky and T. W. Vanderah, "Therapeutic potential of peroxynitrite decomposition catalysts: a patent review," *Expert Opinion on Therapeutic Patents*, vol. 25, no. 4, pp. 443–466, 2015.

[5] R. Radi, "Oxygen radicals, nitric oxide, and peroxynitrite: redox pathways in molecular medicine," *Proceedings of the National Academy of Sciences*, vol. 115, no. 23, pp. 5839–5848, 2018.

[6] G. Ferrer-Sueta, M. Trujillo, S. Bartesaghi, N. Romero, B. Alvarez, and R. Radi, "Biochemistry of peroxynitrite and protein tyrosine nitration," *Chemical reviews*, vol. 118, no. 3, pp. 1338–1408, 2018.

[7] Z. Rajic, A. Tovmasyan, I. Spasojevic et al., "A new SOD mimic, Mn(III) _ortho N_ -butoxyethylpyridylporphyrin, combines superb potency and lipophilicity with low toxicity," *Free Radical Biology and Medicine*, vol. 52, no. 9, pp. 1828–1834, 2012.

[8] Z. Rajic, A. Tovmasyan, O. L. de Santana et al., "Challenges encountered during development of Mn porphyrin-based, potent redox- active drug and superoxide dismutase mimic, MnTnBuOE-2-PyP^{5+}, and its alkoxyalkyl analogues," *Journal of Inorganic Biochemistry*, vol. 169, pp. 50–60, 2017.

[9] S. C. Gad, D. W. Sullivan, J. D. Crapo, and C. B. Spainhour, "A nonclinical safety assessment of MnTE-2-PyP, a manganese porphyrin," *International Journal of Toxicology*, vol. 32, no. 4, pp. 274–287, 2013.

[10] S. C. Gad, D. W. Sullivan Jr., C. V. Mujer, C. B. Spainhour, and J. D. Crapo, "Nonclinical safety and toxicokinetics of MnTE-2-PyP (BMX-010), a topical agent in phase 2 trials for psoriasis and atopic dermatitis," *International Journal of Toxicology*, vol. 38, no. 4, pp. 291–302, 2019.

[11] S. C. Gad, D. W. Sullivan Jr., I. Spasojevic, C. V. Mujer, C. B. Spainhour, and J. D. Crapo, "Nonclinical safety and toxicokinetics of MnTnBuOE-2-PyP5+ (BMX-001)," *International Journal of Toxicology*, vol. 35, no. 4, pp. 438–453, 2016.

[12] I. Batinic-Haberle, Z. Rajic, A. Tovmasyan et al., "Diverse functions of cationic Mn(III) _N_ -substituted pyridylporphyrins, recognized as SOD mimics," *Free Radical Biology and Medicine*, vol. 51, no. 5, pp. 1035–1053, 2011.

[13] I. Batinić-Haberle, A. Tovmasyan, and I. Spasojević, "Mn porphyrin-based redox-active therapeutics," in *Redox-Active Therapeutics*, I. Batinic-Haberle, J. S. Rebouças, and I. Spasojevic, Eds., pp. 165–212, Cham, Springer, 2016.

[14] K. Zakeri, D. Narayanan, B. Vikram, G. Evans, C. N. Coleman, and P. G. S. Prasanna, "Decreasing the toxicity of radiation therapy: radioprotectors and radiomitigators being developed by the National Cancer Institute through small business innovation research contracts," *International Journal of Radiation Oncology • Biology • Physics*, vol. 104, no. 1, pp. 188–196, 2019.

[15] I. Batinic-Haberle and M. E. Tome, "Thiol regulation by Mn porphyrins, commonly known as SOD mimics," *Redox Biology*, vol. 25, 2019.

[16] K. Lee, M. M. Briehl, A. P. Mazar et al., "The copper chelator ATN-224 induces peroxynitrite-dependent cell death in hematological malignancies," *Free Radical Biology and Medicine*, vol. 60, pp. 157–167, 2013.

[17] I. Batinić-Haberle, J. S. Rebouças, L. Benov, and I. Spasojević, "Chemistry, biology and medical effects of water-soluble metalloporphyrins," in *Handbook of Porphyrin Science*, K. Kadish, K. Smith, and R. Guilard, Eds., pp. 291–393, World Scientific Publishing Co. Pte Ltd, Singapore, 2011.

[18] A. Tovmasyan, J. S. Reboucas, and L. Benov, "Simple biological systems for assessing the activity of superoxide dismutase mimics," *Antioxidants and Redox Signaling*, vol. 20, no. 15, pp. 2416–2436, 2014.

[19] A. Vincent, M. Thauvin, E. Quévrain et al., "Evaluation of the compounds commonly known as superoxide dismutase and catalase mimics in cellular models," *Journal of Inorganic Biochemistry*, vol. 219, article 111431, 2021.

[20] A. M. Barbosa, J. F. Sarmento-Neto, J. E. R. Menezes Filho et al., "Redox-active drug, MnTE-2-PyP5+, prevents and treats cardiac arrhythmias preserving heart contractile function," *Oxidative Medicine and Cellular Longevity*, vol. 2020, 15 pages, 2020.

[21] B. Griess, S. Mir, K. Datta, and M. Teoh-Fitzgerald, "Scavenging reactive oxygen species selectively inhibits M2 macrophage polarization and their pro-tumorigenic function in part, via Stat3 suppression," *Free Radical Biology and Medicine*, vol. 147, pp. 48–60, 2020.

[22] A. Tovmasyan, J. C. Bueno-Janice, M. C. Jaramillo et al., "Radiation-mediated tumor growth inhibition is significantly enhanced with redox-active compounds that cycle with ascorbate," *Antioxidants and Redox Signaling*, vol. 29, no. 13, pp. 1196–1214, 2018.

[23] Y. Yang, Q. Wang, J. Luo et al., "Superoxide dismutase mimic, MnTE-2-PyP enhances rectal anastomotic strength in rats after preoperative chemoradiotherapy," *Oxidative Medicine and Cellular Longevity*, vol. 2020, 11 pages, 2020.

[24] Y. Yang, P. Zhang, R. Yan et al., "MnTE-2-PyP attenuates TGF-β-induced epithelial-mesenchymal transition of colorectal cancer cells by inhibiting the Smad2/3 signaling pathway," *Oxidative Medicine and Cellular Longevity*, vol. 2019, 11 pages, 2019.

[25] Y. Zhu, E. A. Kosmacek, A. Chatterjee, and R. E. Oberley-Deegan, "Mnte-2-pyp suppresses prostate cancer cell growth via H_2O_2 production," *Antioxidants*, vol. 9, no. 6, 2020.

[26] I. Spasojević, Y. Chen, T. J. Noel et al., "Pharmacokinetics of the potent redox-modulating manganese porphyrin, MnTE-2-PyP^{5+}, in plasma and major organs of B6C3F1 mice," *Free Radical Biology and Medicine*, vol. 45, no. 7, pp. 943–949, 2008.

[27] T. Weitner, I. Kos, H. Sheng et al., "Comprehensive pharmacokinetic studies and oral bioavailability of two Mn porphyrin-based SOD mimics, MnTE-2-PyP^{5+} and MnTnHex-2-PyP^{5+}," *Free Radical Biology and Medicine*, vol. 58, pp. 73–80, 2013.

[28] V. H. A. Pinto, D. CarvalhoDa-Silva, J. L. M. S. Santos et al., "Thermal stability of the prototypical Mn porphyrin-based superoxide dismutase mimic and potent oxidative-stress redox modulator Mn(III) _meso_ -tetrakis(_N_ -ethylpyridinium-2-yl)porphyrin chloride, MnTE-2-PyP^{5+}," *Journal of Pharmaceutical and Biomedical Analysis*, vol. 73, pp. 29–34, 2013.

[29] A. Tovmasyan, C. G. C. Maia, T. Weitner et al., "A comprehensive evaluation of catalase-like activity of different classes

of redox-active therapeutics," *Free Radical Biology and Medicine*, vol. 86, pp. 308–321, 2015.

[30] A. Tovmasyan, R. S. Sampaio, M. K. Boss et al., "Anticancer therapeutic potential of Mn porphyrin/ascorbate system," *Free Radical Biology and Medicine*, vol. 89, pp. 1231–1247, 2015.

[31] World Health Organization, "WHO guidelines on stability testing of active pharmaceutical ingredients and finished pharmaceutical products," *WHO Technical Report Series 1010*, World Health Organization, Geneva, 2018, https://cdn.who.int/media/docs/default-source/medicines/norms-and-standards/guidelines/regulatory-standards/trs1010-annex10-who-stability-testing-of-active-pharmaceutical-ingredients.pdf?sfvrsn=7cb7a4c9_4&download=true.

[32] D. Jelić, "Thermal stability of amorphous solid dispersions," *Molecules*, vol. 26, no. 1, p. 238, 2021.

[33] World Health Organization, *WHO Expert Committee on Specifications for Pharmaceutical Preparations*, World Health Organization, Geneva, 2018, May 2021, http://www.who.int/medicines/areas/quality_safety/quality_assurance/expert_committee/trs_1010/en/.

[34] M. A. de Oliveira, M. I. Yoshida, and E. C. de Lima Gomes, "Thermal analysis applied to drugs and pharmaceutical formulations in pharmaceutical industry," *Quimica Nova*, vol. 34, no. 7, pp. 1224–1230, 2011.

[35] V. H. A. Pinto, N. K. S. M. Falcão, J. C. Bueno-Janice, I. Spasojević, I. Batinić-Haberle, and J. S. Rebouças, "Cytochrome P450-like biomimetic oxidation catalysts based on Mn porphyrins as redox modulators," in *Redox-Active Therapeutics*, I. Batinic-Haberle, J. S. Rebouças, and I. Spasojevic, Eds., pp. 213–243, Cham, Springer, 2016.

[36] M. C. Jaramillo, M. M. Briehl, J. D. Crapo, I. Batinic-Haberle, and M. E. Tome, "Manganese porphyrin, MnTE-2-PyP 5+, acts as a pro-oxidant to potentiate glucocorticoid-induced apoptosis in lymphoma cells," *Free Radical Biology and Medicine*, vol. 52, no. 8, pp. 1272–1284, 2012.

[37] I. Spasojevic, I. Kos, L. T. Benov et al., "Bioavailability of metalloporphyrin-based SOD mimics is greatly influenced by a single charge residing on a Mn site," *Free Radical Research*, vol. 45, no. 2, pp. 188–200, 2011.

[38] J. M. Pollard, J. S. Reboucas, A. Durazo et al., "Radioprotective effects of manganese-containing superoxide dismutase mimics on ataxia-telangiectasia cells," *Free Radical Biology and Medicine*, vol. 47, no. 3, pp. 250–260, 2009.

[39] M. Blessy, R. D. Patel, P. N. Prajapati, and Y. K. Agrawal, "Development of forced degradation and stability indicating studies of drugs - a review," *Journal of Pharmaceutical Analysis*, vol. 4, no. 3, pp. 159–165, 2014.

[40] ICH Expert Working Group, *Pharmaceutical development Q8(R2)*, 2009.

[41] A. Khawam and D. R. Flanagan, "Basics and applications of solid-state kinetics: a pharmaceutical perspective," *Journal of Pharmaceutical Sciences*, vol. 95, no. 3, pp. 472–498, 2006.

[42] N. Ren, F. Wang, J. Zhang, and X. Zheng, "Progress in thermal analysis kinetics," *Wuli Huaxue Xuebao/ Acta Physico - Chimica Sinica*, vol. 36, no. 6, 2020.

[43] S. Vyazovkin and C. A. Wight, "Model-free and model-fitting approaches to kinetic analysis of isothermal and nonisothermal data," *Thermochimica Acta*, vol. 340–341, pp. 53–68, 1999.

[44] S. Vyazovkin, "Advanced isoconversional method," *Journal of Thermal Analysis*, vol. 49, no. 3, pp. 1493–1499, 1997.

[45] S. Vyazovkin, A. K. Burnham, J. M. Criado, L. A. Pérez-Maqueda, C. Popescu, and N. Sbirrazzuoli, "ICTAC Kinetics Committee recommendations for performing kinetic computations on thermal analysis data," *Thermochimica Acta*, vol. 520, no. 1–2, pp. 1–19, 2011.

[46] S. Vyazovkin, A. K. Burnham, L. Favergeon et al., "ICTAC Kinetics Committee recommendations for analysis of multi-step kinetics," *Thermochimica Acta*, vol. 689, p. 178597, 2020.

[47] S. Vyazovkin, K. Chrissafis, M. L. di Lorenzo et al., "ICTAC Kinetics Committee recommendations for collecting experimental thermal analysis data for kinetic computations," *Thermochimica Acta*, vol. 590, pp. 1–23, 2014.

[48] R. C. O. Sebastião, J. P. Braga, and M. I. Yoshida, "Competition between kinetic models in thermal decomposition: analysis by artificial neural network," *Thermochimica Acta*, vol. 412, no. 1–2, pp. 107–111, 2004.

[49] R. C. O. Sebastião, J. P. Braga, and M. I. Yoshida, "Artificial neural network applied to solid state thermal decomposition," *Journal of Thermal Analysis and Calorimetry*, vol. 74, no. 3, pp. 811–818, 2003.

[50] M. B. F. Marques, B. C. R. Araujo, C. Fernandes, M. I. Yoshida, W. N. Mussel, and R. C. O. Sebastião, "Kinetics of lumefantrine thermal decomposition employing isoconversional models and artificial neural network," *Journal of the Brazilian Chemical Society*, vol. 31, no. 3, pp. 512–522, 2020.

[51] L. D. Ferreira, F. S. Medeiros, B. C. Araujo et al., "Kinetic study of MWCNT and MWCNT@P3HT hybrid thermal decomposition under isothermal and non-isothermal conditions using the artificial neural network and isoconversional methods," *Thermochimica Acta*, vol. 676, pp. 145–154, 2019.

[52] C. R. G. Silva, S. Fialho, J. Barbosa et al., "Compatibility by a nonisothermal kinetic study of azathioprine associated with usual excipients in the product quality review process," *Journal of the Brazilian Chemical Society*, vol. 32, no. 3, pp. 638–651, 2021.

[53] J. S. Rebouças, M. E. M. D. de Carvalho, and Y. M. Idemori, "Perhalogenated 2-pyridylporphyrin complexes: synthesis, self-coordinating aggregation properties, and catalytic studies," *Journal of Porphyrins and Phthalocyanines*, vol. 6, no. 1, pp. 50–57, 2002.

[54] J. S. Rebouças, I. Spasojević, and I. Batinić-Haberle, "Quality of potent Mn porphyrin-based SOD mimics and peroxynitrite scavengers for pre-clinical mechanistic/therapeutic purposes," *Journal of Pharmaceutical and Biomedical Analysis*, vol. 48, no. 3, pp. 1046–1049, 2008.

[55] J. S. Rebouças, I. Kos, Z. Vujasković, and I. Batinić-Haberle, "Determination of residual manganese in Mn porphyrin-based superoxide dismutase (SOD) and peroxynitrite reductase mimics," *Journal of Pharmaceutical and Biomedical Analysis*, vol. 50, no. 5, pp. 1088–1091, 2009.

[56] L. A. Pérez-Maqueda and J. M. Criado, "The accuracy of Senum and Yang's approximations to the Arrhenius integral," *Journal of Thermal Analysis and Calorimetry*, vol. 60, no. 3, pp. 909–915, 2000.

[57] W. Munroe, C. Kingsley, A. Durazo et al., "Only one of a wide assortment of manganese-containing SOD mimicking compounds rescues the slow aerobic growth phenotypes of both _Escherichia coli_ and _Saccharomyces cerevisiae_ strains lacking superoxide dismutase enzymes," *Journal of Inorganic Biochemistry*, vol. 101, no. 11–12, pp. 1875–1882, 2007.

[58] P. I. C.-o. Scheme, *Guide to Good Manufacturing Practice for Medicinal Products (PE 009-15 Part I)*, 2021, May 2021, https://picscheme.org/docview/4205.

[59] A. Khawam and D. R. Flanagan, "Solid-state kinetic models: basics and mathematical fundamentals," *Journal of Physical Chemistry B*, vol. 110, no. 35, pp. 17315–17328, 2006.

[60] M. I. Yoshida, E. C. Lima Gomes, C. D. Vianna Soares, and M. A. Oliveira, "Thermal behavior study and decomposition kinetics of amiodarone hydrochloride under isothermal conditions," *Drug Development and Industrial Pharmacy*, vol. 37, no. 6, pp. 638–647, 2011.

[61] *ICH topic Q 1 A (R2) stability testing of new drug substances and products. Step 5. Note for guidance on stability testing: stability testing of new drug substances and products*, 2003, November 2021, https://www.ema.europa.eu/en/documents/scientific-guideline/ich-q-1-r2-stability-testing-new-drug-substances-products-step-5_en.pdf.

[62] U. Markens, "Conducting stability studies - recent changes to climatic zone IV," *Life Science Services SGS Technical Bulletin*, no. 13, pp. 1–4, 2009, https://www.sgs.com/~/media/global/documents/technical%20documents/sgs%20stability%20studies-en-09.pdf.

[63] L. Benov, "Photodynamic therapy: current status and future directions," *Medical Principles and Practice*, vol. 24, pp. 14–28, 2015.

[64] O. S. Viana, M. S. Ribeiro, A. C. D. Rodas, J. S. Rebouças, A. Fontes, and B. S. Santos, "Comparative study on the efficiency of the photodynamic inactivation of Candida albicans using CdTe quantum dots, Zn(II) porphyrin and their conjugates as photosensitizers," *Molecules*, vol. 20, no. 5, pp. 8893–8912, 2015.

[65] C. G. Andrade, R. C. B. Q. Figueiredo, K. R. C. Ribeiro et al., "Photodynamic effect of zinc porphyrin on the promastigote and amastigote forms of Leishmania braziliensis," *Photochemical and Photobiological Sciences*, vol. 17, no. 4, pp. 482–490, 2018.

[66] T. H. Souza, C. G. Andrade, F. V. Cabral et al., "Efficient photodynamic inactivation of Leishmania parasites mediated by lipophilic water-soluble Zn(II) porphyrin ZnTnHex-2-PyP4 +," *Biochimica et Biophysica Acta (BBA)-General Subjects*, vol. 1865, no. 7, article 129897, 2021.

[67] T. H. Souza, J. F. Sarmento-Neto, S. O. Souza et al., "Advances on antimicrobial photodynamic inactivation mediated by Zn(II) porphyrins," *Journal of Photochemistry and Photobiology C: Photochemistry Reviews*, vol. 49, article 100454, 2021.